Hindawi
Advances in Civil Engineering
Volume 2022, Article ID 9847213, 1 page
https://doi.org/10.1155/2022/9847213

Retraction

Retracted: Fatigue Performance of Reinforced Concrete T-Girders under Cyclic Loading

Advances in Civil Engineering

Received 1 February 2022; Accepted 1 February 2022; Published 11 March 2022

Advances in Civil Engineering has retracted the article titled "Fatigue Performance of Reinforced Concrete T-Girders under Cyclic Loading" [1], due to concerns regarding the reliability of the data as raised by the authors. Following the publication of the article, the authors contacted the journal to raise concerns that the loading instrument used in the experiment was found to be faulty in a recent maintenance check. The load error was found to be over the tolerance of this study. The authors have reviewed the data in the study and note an abnormal trend in Figure 10(b), where the rebar stress range of F-4 decreased after 80% of the life. The remaining data cannot be validated due to the instrument fault.

As the validity of the data presented in the article cannot be verified, the authors requested the retraction of the article and this has been agreed with the editorial board.

References

[1] J. Zhang, B. Bai, K. Zhang et al., "Fatigue Performance of Reinforced Concrete T-Girders under Cyclic Loading," *Advances in Civil Engineering*, vol. 2021, Article ID 6656948, 12 pages, 2021.

Hindawi
Advances in Civil Engineering
Volume 2021, Article ID 6656948, 12 pages
https://doi.org/10.1155/2021/6656948

Research Article

Fatigue Performance of Reinforced Concrete T-Girders under Cyclic Loading

Jinquan Zhang,[1] Bing Bai,[1] Kechao Zhang,[2,3] Shoushan Cheng,[1] Shangchuan Zhao,[1] Lei Wang,[1] and Chenxu Zhuang[1]

[1]*Bridge and Tunnel Research Center, Research Institute of Highway Ministry of Transport, Beijing 100088, China*
[2]*School of Civil Engineering, Chongqing University, Chongqing 400044, China*
[3]*Digital Engineering Department, China-Road Transportation Verification & Inspection Hi-Tech Co., Ltd., Beijing 100088, China*

Correspondence should be addressed to Kechao Zhang; kechao.zhang@ctvic.cn

Received 26 December 2020; Revised 8 March 2021; Accepted 13 March 2021; Published 25 March 2021

Academic Editor: Lingzhi Li

This paper examines the performance of reinforced concrete girders under cyclic loading. Seven T-girders were casted and tested. All girders were loaded under different constant cyclic loading in the midspan with the load ratio of 0.14~0.23 and frequency of 3~4 Hz. The study shows that the longitudinal reinforcement fracture is the main cause of girder rupture. And during cyclic loading, the concrete cracks, strains, and deflections generally indicate a "three-stage" law. The measured data were small but developed quickly in the initial stage. Thereafter, the degradation gradually stabilized and continued for a long time. In the final stage, the cracks, strains, and stiffness degradation developed sharply and the girders failed quickly. The duration of the stage is very short and may be difficult to be caught. For the life estimation, the longitudinal rebar *S-N* curve is fitted using different collected data. The results show that the curve is in good agreement with the corresponding data, which may be an excellent candidate for the evaluation of fatigue life.

1. Introduction

The reinforced concrete T-girders are extensively used in China's highway bridges at present. However, many of them are subjected to a high number of load cycles over the service life. This is also a potential cause of the structural short service life problem. Therefore, fatigue of the concrete girder is an increasingly interesting subject due to the fact that it is a continuous and progressive degradation process, and many high-performance construction materials [1–4] are developed for better antifatigue performance. On account of this issue, China's Technical Standard of Highway Engineering (JTG B01-2014) [5] published in 2014 presented a clear requirement for the life design of bridges.

Despite of all these expectation and material advancement [6, 7], there is still a lack of verification methods dealing with the fatigue life design in current Chinese specifications or standards. The influence of fatigue on the reinforced concrete is not completely understood. As a result, the life design requirement is not fully implemented.

Focusing on this issue, ACI began to study the concrete fatigue problems in 1970s [8, 9] and published some beneficial guidelines on the limit for fatigue-induced stress. In recent discussions, some new tests and points on fatigue-induced failure modes have been studied in depth. Barnes and Mays [10] carried out fatigue tests on five reinforced concrete girders, and they showed that the fatigue fracture of the tensile reinforcement was the dominant factor governing the failure mode, and the fatigue lives of girders were very similar to each other as long as the rebar stress ranges were comparable. Heffernan and Erki [11] studied the fatigue performance of twelve girders with 3 m spans at 3 different load amplitudes and three 5 m span girders, respectively. The result showed that all specimens still failed primarily as a result of brittle fracture of tensile rebars, and only reinforcement with the carbon fiber plate (CFRP) significantly increased the fatigue life because of lower stresses in rebars. These two studies clearly demonstrate that the brittle fracture of longitudinal rebars is the primary mode for fatigue-induced failure, and rebar stress ranges show great influence on the lives. However,

the above findings are obtained from small-scale specimens, and life estimation is not fully involved. In order to investigate the fatigue behavior of larger-scale girders, Charalambidi et al. [12] reported seven large-sized reinforced concrete girder tests with rectangular or T-shaped cross sections. The study showed that all girders subjected to high-amplitude loading failed primarily due to the tensile fracture of the steel rebars, which indicates no mode change for different specimen sizes. And, the fatigue life was found increasing as the ratio of strengthened FRP stiffness to steel stiffness increased. This provides a guidance for the life extension design of the structures, which is of innovation. In addition, Mirzazadeh et al. [13] investigated the fatigue performance of reinforced concrete girders at different temperatures and studied the failure mode and stiffness change law. The results showed that the low temperatures might have a beneficial impact on their fatigue lives. And, these improvements occurred because of the higher strength of the concrete and lower stresses in the tensile reinforcement at low temperature. The findings are rarely explored and of novelty, which is of interest for the maintenance of bridges in cold regions. Gheorghiu et al. [14] performed fatigue tests on thirteen small-scale concrete girders. The results demonstrated that energy dissipation due to the progressive microcracking was great in the initial cycles, and the increase rate of deflection or stiffness degradation became remarkably slower after about 1 million cycles. The study conducted by Ekenel et al. [15] investigated the effect of fatigue on flexural residual capacity of girders. The results showed that the repeated loading caused the girder ductility to decrease about 18% and stiffness degradation occurred in the first 0.5 million cycles. Both the two studies demonstrate that the fatigue evolution proceeds in a multistage law, and the cracks and stiffness degradation increase rates vary in different stages. The approaches may be of interest for the damage accumulation evaluation. In China, similar tests [16–18] have also been conducted to investigate the fatigue performance of reinforced concrete girders. Nevertheless, deeper studies are necessary regarding the cyclic behavior of girders casted in the same batch. In addition, the reinforcement material and design principles in early studies may differ to that of the current condition. For these reasons, the reinforced concrete girder failure mechanism, life estimation, and evolution of cracks and stiffness degradation are still lacking of understanding in spite of the high demand for structural long service life in recent years.

To address this lack of knowledge, this paper presents an investigation into the fatigue life and behavior of seven large-scale conventionally reinforced concrete girders. The failure mode and mechanism are deeply discussed, and a detailed "three-stage" evolution law of cracks, concrete and rebar strains, and degradation of stiffness over the number of cycles are presented. The *S-N* curve for rebars embedded in concrete is also proposed and discussed for life estimation using the data collected from both this study and others, which are of originality. The study is essential to understand the fatigue behavior of large-scale reinforced concrete members and is of particular importance to the bridge life design.

2. Design and Test Scheme of Girders

2.1. Design of Test Girders. Specimen details were chosen to correspond to the major type of medium-span bridges, and reinforced concrete T-girders were chosen as the test specimens. Nine girders with 4500 mm spans were casted in the same batch. Two of them were tested to failure to determine the static bearing capacity, and the remaining girders were subjected to the different levels of cyclic loading.

The manufacturing length of test girders was 5000 mm. And, the cross section was T-shaped without a horseshoe. The depth of the girders was 370 mm with flange width of 500 mm. The web had a constant thickness of 120 mm. Concrete mixes were designed with the compressive strength grade of C40 according to the Chinese Code for Design of Concrete Structures [19], while the actual strength was 50.1 MPa in average according to the cubic specimen test. For the reinforcement, 12 mm in diameter hot-rolled rebars in grade HRB335 (yield strength was 441.8 MPa) were provided as the longitudinal tensile rebars, and 8 mm in diameter round bars in grade R235 (yield strength was 335 MPa) were used as vertical reinforcement and stirrups with spacing of 200 mm. The net protective layer thickness was designed to be 30 mm to avoid the potential environmental erosion. The detailed sketch of the girders is shown in Figure 1. With the reinforcement check calculation, the test girder reinforcement ratio ρ was 0.66%, which met the requirement of the reinforcement ratio ($\rho_{\min} = 0.29\% < \rho < \rho_{\max} = 1.6\text{~}1.8\%$) defined by the Chinese Code for Design of Concrete Structures [19]. The material strengths of both concrete and reinforcing steel are shown in Table 1.

2.2. Testing Program. The program adopted involved testing both the static failure load and fatigue behavior. 2 of the 9 girders were loaded statically to failure to determine the ultimate bearing capacity. Thereafter, the remaining 7 girders were tested by the constant amplitude cyclic loading. The valleys of the loading were determined to be 5 kN to correspond to the effect of deck pavement weight. And, the ranges of cyclic loads were chosen to be 12.5, 16, 17, 19.5, 23, and 30 kN, respectively. The range of 19.5 kN was determined to correspond to the effect of vehicle load defined by China's Technical Standard of Highway Engineering (JTG B01-2014) [5]. And, the range of 30 kN was approximately accounted for 1.5 times of the vehicle overload effect and half of the ultimate failure load. The range levels of 12.5~23 kN were chosen to correspond to the effects of different service states and 25~40% of the total failure load.

The structural fatigue is mainly caused by the repeated action of vehicles; especially, in medium- and short-span bridges, the effects of single wheel or axial load function are notable. On account of this, all of the girders were loaded under single-point bending in the midspan. The loading form was also widely used in previous studies [20, 21]. The load was applied with a PMW-2000 electro-hydraulic pulsating fatigue actuator with the maximum capacity of

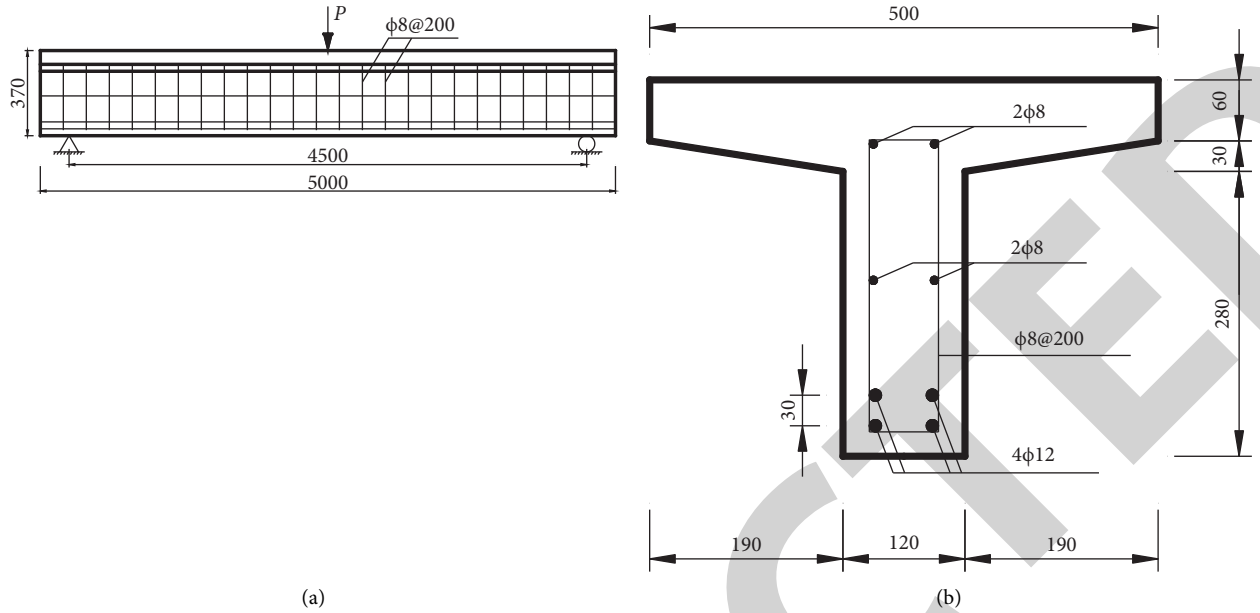

Figure 1: Geometry of the test girders (unit: mm).

Table 1: Girder material test result.

Material	Test result		
Concrete	Compressive strength (MPa)		
C40	50.1		
Reinforcement	Diameter (mm)	Yield strength (MPa)	Ultimate strength (MPa)
Longitudinal bar	12	441.8	606.3
Stirrup	8	335.0	526.8

1000 kN and error of 1 kN. The actuator was connected to the loading frame to transmit the load to the foundation. The loading layout of the test girder is shown in Figure 2.

The static test was firstly conducted to obtain the ultimate failure load and serve as reference for the fatigue tests. Then, the fatigue tests of 7 T-girders were carried out with different load ranges, respectively. The load range for each specimen was kept constant all through the test. The detailed procedures are described as follows:

(1) Static test: 2 girders were loaded under single-point bending in Figure 2, until the specimen failed. Record the load value Pu (mean $Pu = 70$ kN) and unload.

(2) Fatigue case I: ① the specimen was loaded statically to obtain the initial cracks and strains and deflections for record; ② determine the load range $P_{\min} \sim P_{\max}$ and apply the cyclic loading to the specimen in the same loading form; ③ at regular intervals of cycle numbers ($N = 10^4$, 6×10^4, 16×10^4, and 10^5 cycles' intervals thereafter), conduct a static test with the maximum load value of $P_{\max}$, and the purpose is to obtain the evolution of structural degradation with the increase of cycle numbers; ④ resume cyclic loading and repeat steps ②~③ until the final failure of test girders.

(3) Fatigue case II ~ VII: change the load range and conduct the fatigue tests of the remaining 6 girders in the same procedures of the fatigue case I. The detailed loading parameters for each girder are shown in Table 2.

(4) Failure information record: inspect specimens and record the cycle numbers for each girder after fatigue failure. Determine the failure mode and mechanical evolution.

In order to determine the structural mechanical evolution with the number of loading cycles, the strains, deflections, and concrete cracks were measured using the high-precision sensors and gauges. Four critical sections (1, 2-1, 2-2, and 3, respectively) were selected for concrete strain measurement. And, 13 strain gauges were mounted on each section from the flange to the web for each girder. The reinforcement stresses were also determined from strain gauge readings. The gauges were mounted on the surface of reinforcement prior to casting the girders. Two longitudinal rebars at the bottom were chosen to be measured in 1/4 spans and midspans. In addition, the deflections of girders were continuously measured by the wire-drawn displacement sensors which were mounted near the supports, 1/4 spans, and midspans, respectively. The overall sensor arrangements are shown in Figure 3.

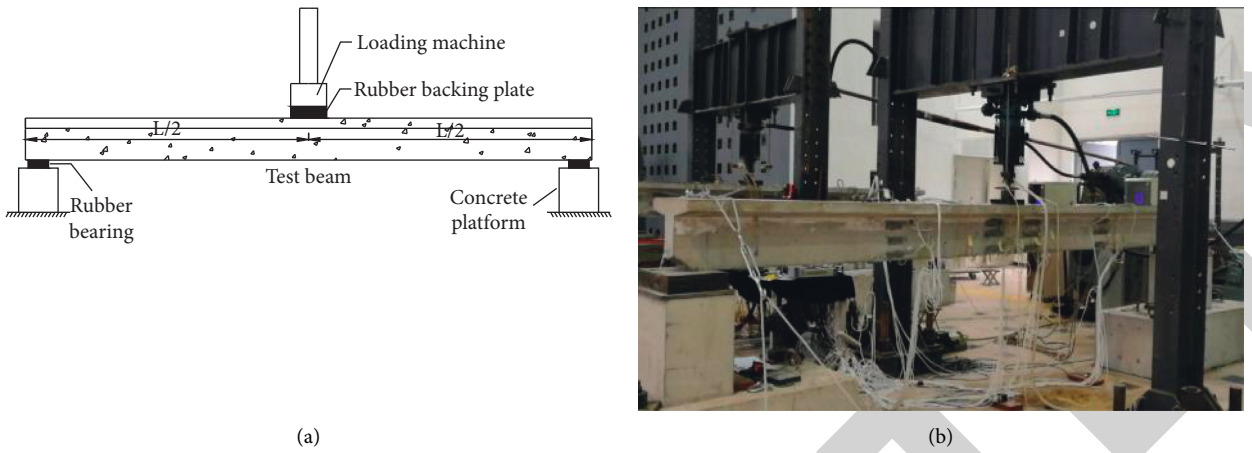

Figure 2: Layout of the test loading. (a) Loading diagram. (b) Photo of the loading layout.

Table 2: Loading parameters of the test.

Test identifier	Loading form	Load range (kN)	Valley value (kN)	Peak value (kN)	Loading frequency (Hz)	Cycles for each static loading
S-1	Static bearing capacity	—	—	$P_{u1} = 77$	—	—
S-2	Static bearing capacity	—	—	$P_{u2} = 63$	—	—
F-1	Constant amplitude fatigue	30	5	$35/0.50P_u$	3	$N = 10^4$, 6×10^4, 16×10^4, and 10^5 cycles intervals thereafter
F-2	Constant amplitude fatigue	23	5	$28/0.40P_u$	3	
F-3	Constant amplitude fatigue	12.5	5	$17.5/0.25P_u$	3.5	
F-4	Constant amplitude fatigue	12.5	5	$17.5/0.25P_u$	4	
F-5	Constant amplitude fatigue	19.5	5	$24.5/0.35P_u$	3	
F-6	Constant amplitude fatigue	16	5	$21/0.30P_u$	3.5	
F-7	Constant amplitude fatigue	17	5	$22/0.31P_u$	3	

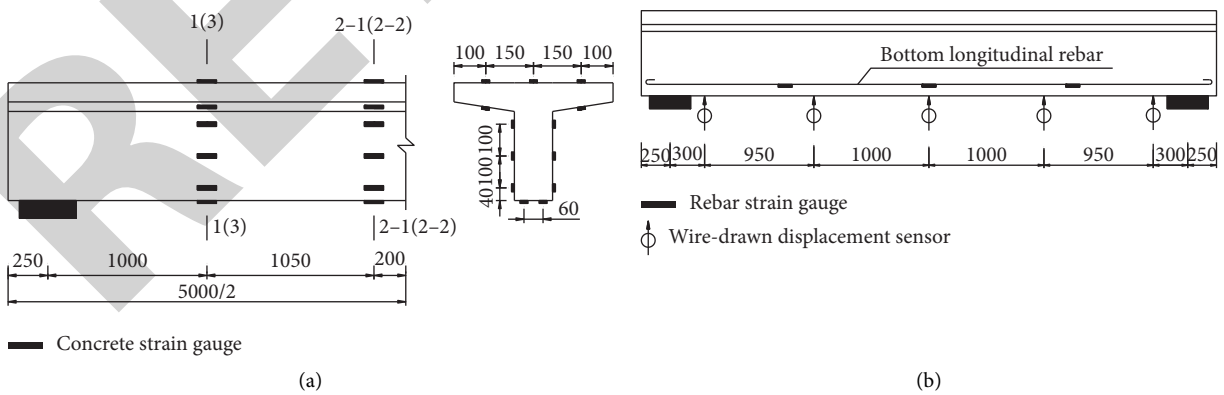

Figure 3: Arrangements of strain gauges and deflection for the test girders (unit: mm). (a) Concrete strain gauge arrangements. (b) Rebar strain gauge and displacement measurement arrangements.

To get the stable sensor readings during different static loading, each load stage was kept for at least 5~15 min. The strains, deflections, as well as crack length and width were then measured to record the damage evolution. The strain and deflection data were acquired by the Kyowa UCAM-60B high-speed strain acquisition instrument. And, crack width

and length were measured using the crack width detector (accuracy: 0.01 mm) and magnifying glass, which is of good accuracy.

3. Test Results

3.1. Fatigue Life and Failure Mode of Girders. The applied load at the midspan on each girder was cycled between the peak and valley value at a rate of 3~4 Hz, which is listed in detail in Table 3. The fatigue lives, leading failure mode, as well as rebar stress ranges obtained from strain gauges are summarized in Table 3. According to the tests, all girders failed due to the cyclic load except the girder F-3. The girder was assumed to show a run out phenomenon after 9 million cycles of fatigue loading. In comparison, the remaining 6 girders all failed at different loading cycles.

According to the test results, except the girder F-3 (run out), the lives of other 6 girders show a negative correlation with the loads or rebar stress ranges. When the loads or stresses got larger, the fatigue lives became smaller. The life for each girder varied from 38.4 thousand to 376.4 thousand cycles and covers the common range of test results in laboratories. In spite of the correlation, the fatigue lives still exhibited considerable deviations due to the material microscopic fatigue mechanism [22]. The applied loads on F-6 and F-7 were very close, while their lives differed greatly. As discussed in the earlier study [22], this phenomenon is largely attributed to the quality difference of rebar micrometallurgical defects or surface conditions. And, the appearance had also been observed in other experimental studies [23].

With regard to the fatigue-induced failure mode, it can be found that the fatigue fracture of longitudinal rebars near the major concrete crack was the leading mode, and it finally led to the bearing capacity loss of the members. The concrete failure is not the main cause of the member loss, which is important to be clarified. The failure process can be described as follows. As the girder was about to fail, the major cracks near the midspan (the number usually was 1~3) continued to expand, while the other cracks gradually closed. In this stage, the major crack width was usually larger than 0.20 mm and developed very quickly. The girder longitudinal rebars finally fractured near the region of major cracks in the midspan, and the number of fractured rebars was usually 2~3. The girders then lost their bearing capacity. During the failure process, it is worth noting that all concrete in compression was not crushed except F-1 on which no displacement limit device was mounted. This phenomenon confirms the finding of Song et al. [24]. The compressive concrete will not fail before the failure of longitudinal reinforcing steel when girders are underreinforced. The postfailure images of F-1 and F-2 are shown in Figure 4, and the other girder failure modes are similar to the latter one.

After tests, the fractured rebars were taken out to inspect the fractured surface details. The surface was plain and smooth in comparison to the ductile failure (yielding and necking, as shown in Figure 5(a)). And, no pronounced deformation or necking was found near the region, which differed greatly from the static failure. In addition to the above, the fractured surface shows an obvious crack growth zone, and the mark confirms the mechanism of metal fatigue fracture [22, 25]. All of the cracks were initiated at the surface of rib root, which happened to be the stress concentration area. This phenomenon is also consistent with the explanation of fracture mechanics [22].

3.2. Structural Crack and Deflection Evolution. In the static tests, a large number of cracks were observed in the concrete tensile zone and the region was assumed to be out of work before cyclic loading, while in fatigue tests, the cracks and deflections would still develop according to the inspection of evolution data.

The test results show that the new cracks are generally initiated within no more than 10% of the entire lives, which can be defined as the initial stage. Thereafter, the crack number and length gradually stabilized, while the width developed slowly. When the specimen was close to failure, the cracks propagated sharply again and finally split because of the rebar fracture. The evolution can be observed in all specimens and is of universality. According to this, the crack evolution process can be summarized as 3 stages: initial stage of rapid development, midterm stable stage, and final failure stage. The major crack width development of each girder is shown in Figure 6.

The initial stage is the crack initiation stage. In this stage, cracks mainly developed with the increase of crack numbers. 1~3 major cracks were initiated generally. After this stage, very few new cracks were found, and the slow propagation of existing cracks dominated. The maximum crack width for each girder ranged from 0.19 to 0.30 mm. But, the value was not consistent with the value of loads. The evolution developed slowly, and the duration was expected to be about 80% of the total lives. The final stage is the near-failure stage. The midspan cracks widened very sharply, while some others began to close. The girders finally failed without any other warnings except some crack closure in the period. Due to the short duration of the final stage, predicting or capturing the failure moment is difficult.

The typical crack distribution in both fatigue and static tests is shown in Figure 7. It can be found that the shear crack distribution in the static test was different from that in fatigue tests. The number of shear cracks accounted for about 50% of the total cracks at static failure girders, while the crack pattern of fatigue failure girders was generally vertical and bending-induced. The shear cracks were less developed, accounting for only 10~20%.

The structural deflection reflects the degradation of girder stiffness. The deflection was measured after every 100,000 cycles, and the evolution results are shown in Figure 8. The test results show that the girder deflection also indicates a "three-stage" law, which is similar to the crack development. In the initial cycles, the deflection was small but changed quickly, and girders were considered at the early stage of cumulative damage. As the cycles increased, the deflection gradually stabilized. The stiffness of test girders at this stage remained almost unchanged and was assumed in a stable state. During the final stage, the structural stiffness

Table 3: Summary of T-girder fatigue failure characteristics.

Girder identifier	Loading frequency (Hz)	Load range (kN)	Rebar stress range (MPa)	Cycles to failure (10^3)	Failure mode
S-1	—	—	—	—	Longitudinal rebar yielding
S-2	—	—	—	—	Longitudinal rebar yielding
F-1	3	5~35	305	384	3 rebars fractured, 1 major crack penetrated the cross section, and the maximum crack width was 20 mm
F-2	3	5~28	230	555	3 rebars fractured, 3 major cracks occurred and penetrated the web at 2.3~2.4 m from the support, and the maximum crack width was 17 mm
F-3	3.5	5~17.5	126	>900,0	Ran out and the static ultimate failure load after 9 million cycles was 64 kN
F-4	4	5~17.5	121	3,401	3 rebars fractured, 1 major crack occurred and penetrated the web at 2.4 m from the support, and the maximum crack width was 7 mm
F-5	3	5~24.5	181	1,123	3 rebars fractured, 2 major cracks occurred and penetrated the web at 2.3 m from the support, and the maximum crack width was 2.9 mm
F-6	3.5	5~21	163	3,764	2 rebars fractured, 1 major crack occurred and penetrated the web at 2.6 m from the support, and the maximum crack width was 13 mm
F-7	3	5~22	170	1,697	3 rebars fractured, 1 major crack occurred and extended to the flange at 2.45 m from the support, and the maximum crack width was 9 mm

(a) (b)

Figure 4: Typical fatigue failure modes of the test girders. (a) F-1 girder fatigue failure mode. (b) F-2 girder fatigue failure mode.

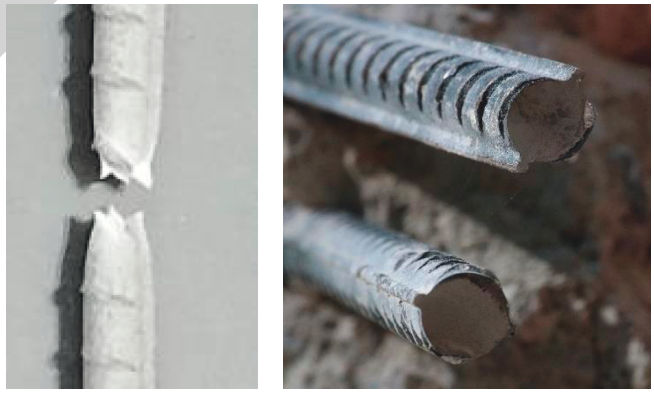

(a) (b)

Figure 5: Fracture morphology comparison between different rebar failure modes. (a) Rebar yield failure. (b) Rebar fatigue failure.

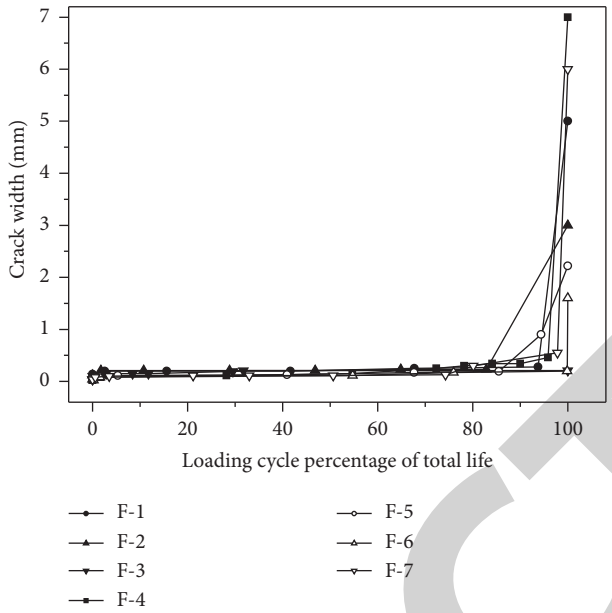

Figure 6: Overall development law of test girder major crack width.

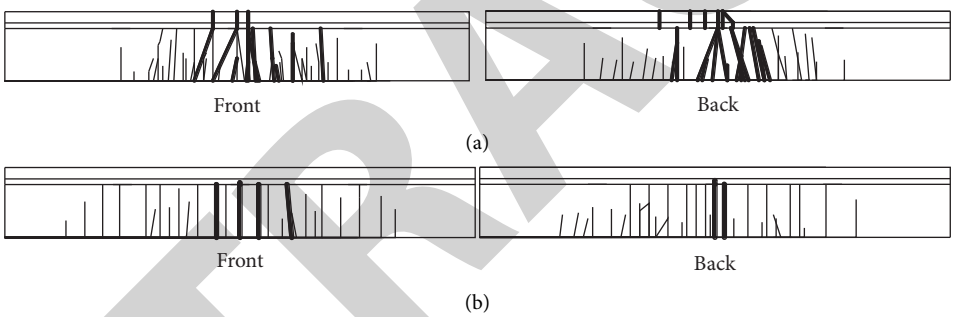

Figure 7: Crack distribution comparison for static and fatigue test girders. (a) S-1 girder crack distribution. (b) F-1 girder crack distribution.

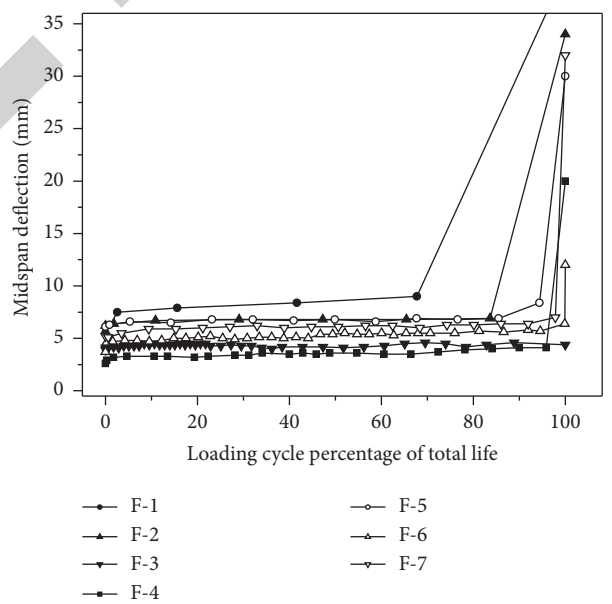

Figure 8: Overall evolution law of test girder deflection.

degraded sharply and led to the rapid increase of deflection until the failure of specimens.

3.3. Concrete Strain Evolution in the Compression Zone. The accuracy of concrete strain measurement is slightly limited due to the material constitutive relation and microcrack development. Despite this, the results still serve as good reference for the evolution. The strain gauges mounted on the flange of the midspan section worked well all over the tests and indicated a highest compressive reading. Figure 9 shows the load-strain curve changes with the increase of cycle numbers. Other evolution curves are similar to this, which will not be repeated.

Figure 9 shows that the load-strain curves moved downward with the increase of cycles, which indicates that greater strain values were observed as cycle numbers increased. The curve corresponding to the first cycle loading is generally located at the top of the whole curves, while, in later stages, say 10,000 cycles, it fell gradually and tended to be stable. As the specimen was to fail, the curve shift rate increased again and gradually deviated from the previous cluster till failure. But, overall, the strain gauge readings measured at each regular interval did not change significantly from others. The maximum variation was only around 10~35 $\mu\varepsilon$. Taking the measurement at 10,000th cycle in the stable period as the example, the difference from this cycle to the subsequent test was even smaller than 20 $\mu\varepsilon$.

Considering the strain development of specimens, it is reasonable to infer that the concrete strain evolution also conforms to the "three-stage" law. In the initial stage of cyclic loading, the concrete strains and cracks developed quickly during the first 10,000 cycles. Then, the response changed slowly in a long period. In the final stage of fatigue lives, the strain increase rate became higher, but the evolution was still not remarkable. Even before failure, most strains and cracks showed no abrupt changes in the last measurement. This reflects from the other side that the duration of structural failure was very short, and no obvious warnings could be caught, which confirms the difficulty of failure capture with regular concrete measurement. Also, another point worth noting is that the change of concrete response may provide little information about the life estimation as the failure is not caused by concrete loss.

3.4. Stress Range Evolution of Longitudinal Reinforcement. The failure mode of longitudinal rebar fracture shows that the stress range of reinforcement may be a key parameter affecting the fatigue performance. In order to obtain the stress evolution of specimens, the strain gauges were mounted on the longitudinal reinforcement before the casting of concrete. And, the readings from the periodic static tests on the specimens were recorded and converted to the stresses.

Figure 10 shows the obtained stress range cycle curves of each girder. The results show that the stress ranges of longitudinal rebars were relatively stable and regular in the initial and midterm stages of cyclic loading. The data show a negative correlation with the fatigue life. However, the stress range of each girder varied in the final stages, which may be an important reason for the difference of life results. The test results suggest the following. ① The rebars in each girder experienced a varying growth of the stress range in the initial stage (no more than 5% of total lives), and then, the values quickly became stable and entered the midterm stage (5%~60% of total lives). In this stage, the growth was very slow and continued for a long time. ② In the later period of loading cycles, there were two forms of stress change for all girders. Except F-4 and F-7, all girder reinforcement continued to remain almost unchanged until last 1~3 measuring times (more than 80% of total lives), while, for girders F-4 and F-7, no subsequent stress stable period was found, and the rebar stresses rose gradually after 60~65% of the total lives. This phenomenon is significant because the stress range evolution process changed greatly in the last 1/3 of the lives. And, the stress range cycle curve pattern was different from others. ③ The girder F-3 did not fail after 9 million cycles. The stress range of it was similar to that of F-4, but their lives were different. In order to explore its capacity, a static loading test (single-point bending form) was conducted after cyclic loading, and its bearing capacity was 64 kN, which suggested no obvious deterioration found in comparison to S-1 and S-2. This run out phenomenon may be attributed to the initial defect freeness of longitudinal reinforcement, good surface treatment, etc. [22], and similar results can be found in other tests [26]. ④ The stress ranges of F-4 and F-7 were relatively stable in their first 65% of lives, which were 116 MPa and 170 MPa, respectively. After the period, a sudden increase was observed when F-4 was loaded for 2.46 million cycles. The stress range increased to 168 MPa and continued to grow slowly. To determine the reasons for the sudden increase, a major crack with 0.25 mm width was found near the strain gauge. And, the crack opening and closure were clearly observed during cyclic loading. The width was measured to be 0.46 mm and extended to the bottom of the flange after 3.26 million cycles. A similar case could also be observed in the F-7 loading process. The rebar stress range immediately changed to about 200 MPa with the rapid development of a major crack at F-7. However, the deflections of the two girders showed no significant changes at the corresponding cycles, which suggested the stiffness was still stable. ⑤ The increase in rebar stress ranges before failure could be detected in almost all cases. This might be due to the severe accumulated damage of longitudinal reinforcement, and the cross section was considered to be reduced. In order to maintain the sectional equilibrium, the concrete and rebar stresses redistributed and led to the excessive deformation. As a result, the control of crack width was weakened and assumed to explain the accompanied ultrawide concrete cracks.

In light of the curves shown in Figure 10, it may also be concluded that the longitudinal rebar stress ranges are better parameters to predict the fatigue lives in comparison to concrete cracks, strains, and deflections. The ranges determined from gauge readings are stable and considered more suitable to evaluate the structural fatigue lives.

4. Discussion on the *S-N* Curve of Reinforcement

The test results show that the rebar stress range is essential for the fatigue life behavior. To predict fatigue lives, it is

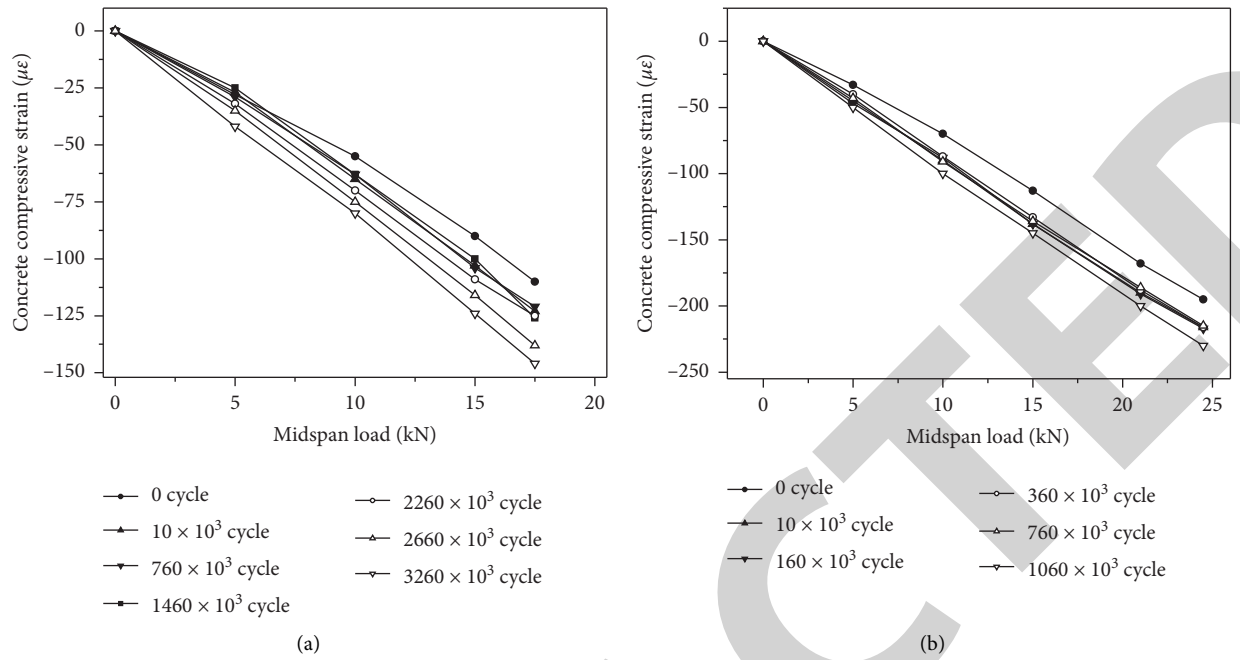

Figure 9: Concrete strain evolution law of typical test girders. (a) Relationship between flange compressive strain and load in the F-4 girder. (b) Relationship between flange compressive strain and load in the F-5 girder.

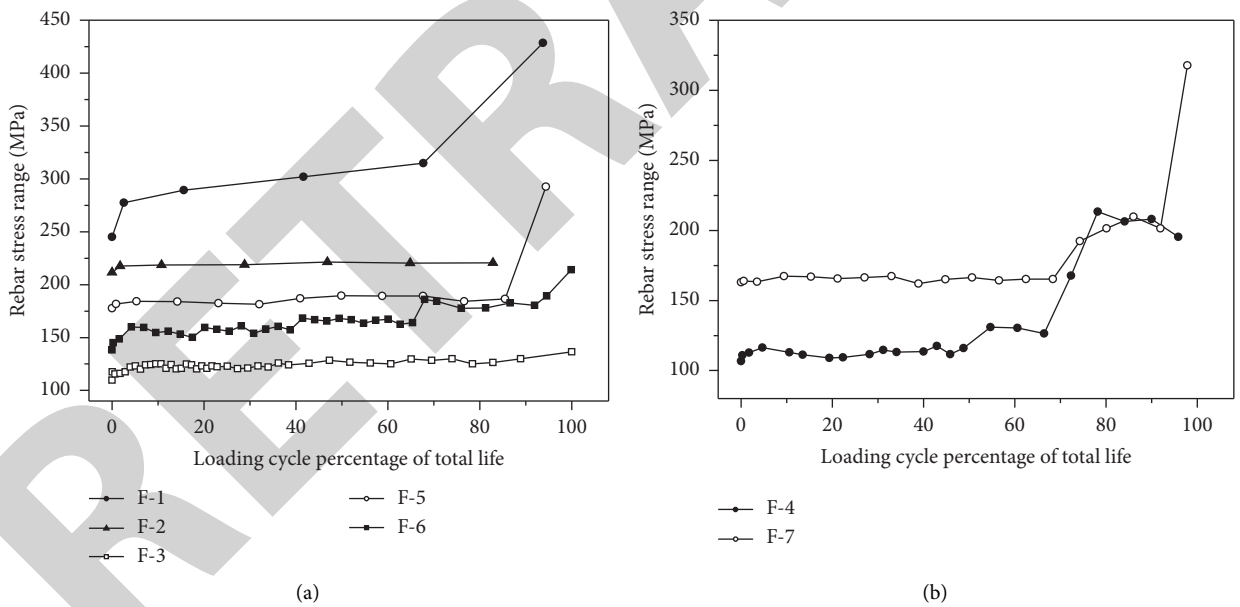

Figure 10: Overall evolution law of longitudinal rebar stress ranges. (a) Relationship between rebar stress ranges and loading cycles for F-1~F-3, F-5, and F-6 girders. (b) Relationship between rebar stress ranges and loading cycles for F-4 and F-7 girders.

necessary to establish the *S-N* (stress range-tested cycle number) curve [25] for longitudinal reinforcement in concrete subjected to cyclic flexure loading.

The *S-N* approach requires fatigue test data to develop the best-fit relationship that describes the life estimation of the material. Figure 11 shows the testing data points of rebar stress ranges and cycles for each specimen. Due to the run out of F-3, there are only 6 pairs of data available in the curve fitting analysis. The corresponding *S-N* curve using the least square method [27, 28] is obtained as follows:

$$\lg N = -2.5946 \lg \Delta\sigma + 12.0050. \quad (1)$$

The curve is a median one with the correlation coefficient $R = 0.912$. Further evaluation for ±2 standard deviations can be obtained by statistics, which is also shown in Figure 11.

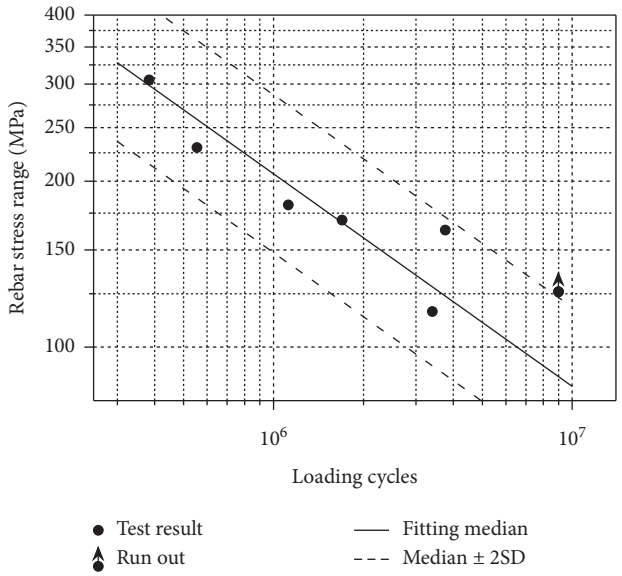

Figure 11: *S-N* data and corresponding linear fitting of this test.

The results show that all the 6 pairs of data fall within the ±2 standard deviations, which suggests that the curve fits well. However, the data are too few to reflect the general rules in spite of the good correlation coefficient. The statistical significance of the curve is still in doubt. More comparison and verification work are necessary to carry out.

To verify the fitted curve, the data from different studies [16, 23, 29] are shown in Figure 12. The comparison suggests that the scatter from different tests varies greatly. The fitted curve is not consistent to other collected data, and many data points fall outside of the ±2 standard deviations, which means the fitting is inappropriate. This problem may also demonstrate that the 6 data-based *S-N* curves have no sufficient statistical significance. All data should be combined together for further investigation.

Collecting all the data from different tests, there are 24 points available for the establishment of the *S-N* curve. The data are calculated for the log-log fitting. And, the corresponding curve is then obtained as

$$\lg N = -2.3577 \lg \Delta\sigma + 11.1809. \quad (2)$$

The correlation coefficient R for the equation is reduced to 0.779. The reduction is actually consistent with the statistical law. In general, the coefficient R decreases with the increase of data quantities. However, the value for the fitting curve is still greater than the threshold $R_{\min} = 0.404$ [28], and the result has statistical significance. The fitting result and test data are shown in Figure 13.

In practice, equation (2) should be modified to consider the redundancy that describes the fatigue life with a reasonable confidence level. The level might be taken as 97.7%, which corresponds to 2 standard deviations downward from the median one. The equation is expressed as

$$\lg N = -2.3577 \lg \Delta\sigma + 10.6309. \quad (3)$$

Inspecting this curve in Figure 13, it can be found that all the points lie above the curve, which demonstrates that the curve fulfils the calibration requirements.

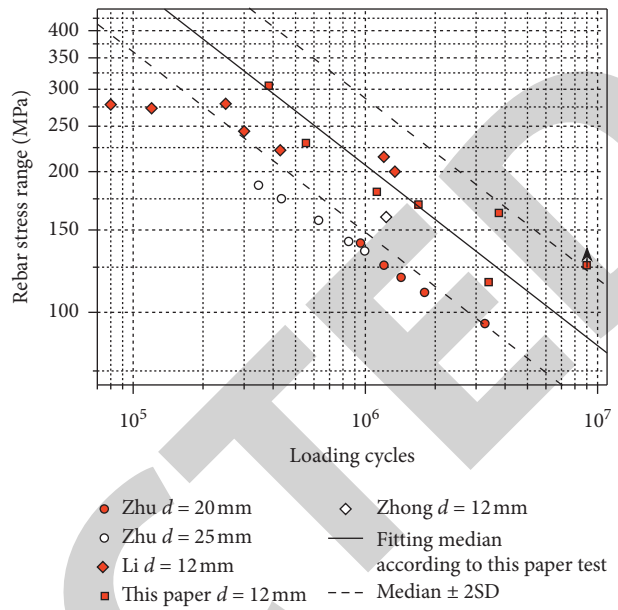

Figure 12: All test (*S-N*) data collection and linear fitting of this test.

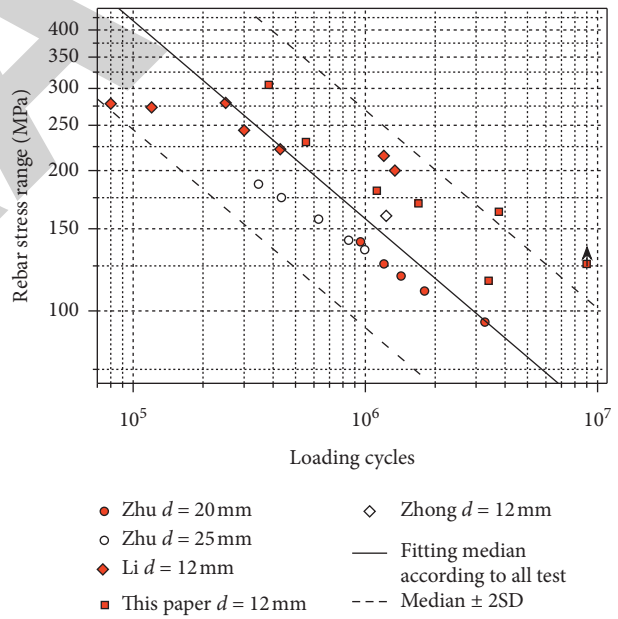

Figure 13: All test (*S-N*) data and corresponding linear fitting.

In order to discuss the curve further, equation (3) and *S-N* relationship prescribed by Eurocode 2 [30] are shown in Figure 14. It can be found from the figure that the curve slope in Eurocode 2 is quite different from equation (3), and the former decreases more slowly. In addition, the curve lies mostly above the fitted -2SD curve, and a considerable number of points are located under it, which suggests that the redundancy is insufficient. The life estimation using the Eurocode 2 curve might lead to the unsafe result, while equation (3) shows good performance compared to the curve prescribed by Eurocode 2. The fitted curve is in very good agreement with the collected data, and the confidence level is reasonable.

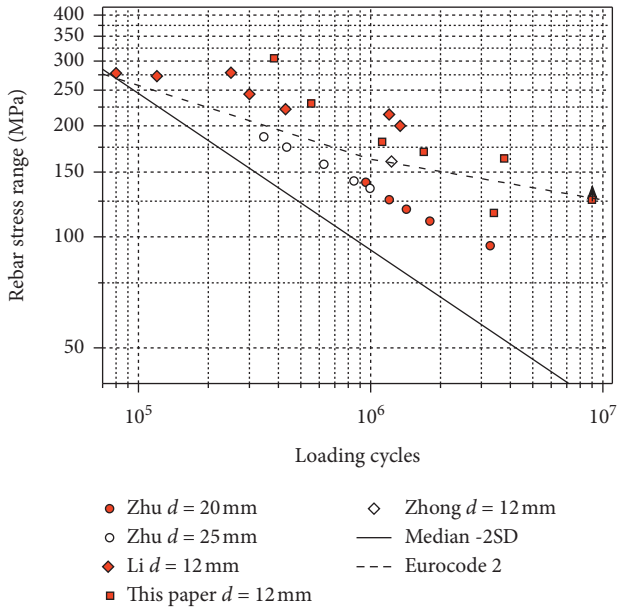

Figure 14: *S-N* curve comparison between equation (3) and Eurocode 2.

5. Conclusions

7 T-girder fatigue tests under different load amplitudes were carried out. The failure mode, mechanical evolution, and *S-N* relationship are discussed based on the test results. The following major findings can be drawn from the study:

(1) The fatigue-induced failure mode is clear. All specimens except F-3 failed in a tension flexural mode due to the fatigue fracture of the longitudinal reinforcement near the midspan. The tensile rebars deformed little, and no obvious warnings were observed before the final fatigue failure of the specimens.

(2) During cyclic loading processes, the concrete cracks and deflections proceed in a "three-stage" law. The measured values in the initial stage developed very quickly, while, in the second stage, the values remained almost unchanged for a long time. The duration may be about 80% of the total lives. When the specimens were to fail, the values increased sharply again and girders failed rapidly.

(3) The concrete strain evolution also follows a "three-stage" law. However, capturing the strain changes at the final stage was difficult because of the short duration of the stage. As concrete did not fail after the girder loss, the evolution of concrete strain may provide little information about the life estimation.

(4) The measured results of the longitudinal rebar stress range are more stable and regular compared to other mechanical parameters. All rebar stress ranges increased in the final stage due to the severe damage and stress redistribution. And, the total evolution shows a strong correlation with the final failure and lives.

(5) The longitudinal reinforcement *S-N* curve is fitted by test results and other collected data. The comparison to Eurocode 2 shows that the obtained curve is in good agreement with the test data and has sufficient redundancy, while the Eurocode 2 curve might lead to an unsafe result. Further investigation based on the curve is needed to establish a life calibration method.

Data Availability

The data used to support the findings of this study are available from the corresponding author upon request.

Conflicts of Interest

The authors declare that there are no conflicts of interest regarding the publication of this paper.

Acknowledgments

This study was funded by the Science and Technology Innovation Foundation of Research Institute of Highway, Ministry of Transport (Grant nos. 2019-I113 and 2018-A0004) and National Key R&D Program of China (Grant no. 2018YFC0809606).

References

[1] A. Ramachandra Murthy, B. L. Karihaloo, P. Vindhya Rani, and D. Shanmuga Priya, "Fatigue behaviour of damaged RC beams strengthened with ultra high performance fibre reinforced concrete," *International Journal of Fatigue*, vol. 116, pp. 659–668, 2018.

[2] H. Ma and Z. Zhang, "Paving an engineered cementitious composite (ECC) overlay on concrete airfield pavement for reflective cracking resistance," *Construction and Building Materials*, vol. 252, Article ID 119048, 2020.

[3] Z. Zhang, F. Yang, J.-C. Liu, and S. Wang, "Eco-friendly high strength, high ductility engineered cementitious composites (ECC) with substitution of fly ash by rice husk ash," *Cement and Concrete Research*, vol. 137, Article ID 106200, 2020.

[4] Z. Zhang, F. Qin, H. Ma, and L. Xu, "Tailoring an impact resistant engineered cementitious composite (ECC) by incorporation of crumb rubber," *Construction and Building Materials*, vol. 262, Article ID 120116, 2020.

[5] JTG B01-2014, *Technical Standard of Highway Engineering*, China Communications Press, Beijing, China, 2014.

[6] F. Qin, Z. Zhang, Z. Yin, J. Di, L. Xu, and X. Xu, "Use of high strength, high ductility engineered cementitious composites (ECC) to enhance the flexural performance of reinforced concrete beams," *Journal of Building Engineering*, vol. 32, Article ID 101746, 2020.

[7] Z. Zhang, Q. Zhang, and V. C. Li, "Multiple-scale investigations on self-healing induced mechanical property recovery of ECC," *Cement and Concrete Composites*, vol. 103, pp. 293–302, 2019.

[8] ACI Committee 215, "Considerations for design of concrete structure subjected to fatigue loading," *ACI Proceedings*, vol. 71, no. 3, pp. 97–121, 1974.

[9] J. O. Holmen, "Fatigue of concrete by constant and variable amplitude loading," *ACI Special Publication*, vol. 75, pp. 71–110, 1979.

[10] R. Barnes and G. Mays, "Fatigue performance of concrete beams strengthened with CFRP plates," *Journal of Composite for Construction*, vol. 3, no. 4, pp. 63–72, 1999.

[11] P. J. Heffernan and M. A. Erki, "Fatigue behavior of reinforced concrete beams strengthened with carbon fiber reinforced plastic laminates," *Journal of Composites for Construction*, vol. 8, no. 2, pp. 132–140, 2004.

[12] B. G. Charalambidi, T. C. Rousakis, and A. I. Karabinis, "Fatigue behavior of large-scale reinforced concrete beams strengthened in flexure with fiber-reinforced polymer laminates," *Journal of Composite for Construction*, vol. 20, no. 5, Article ID 04016035, 2016.

[13] M. M. Mirzazadeh, M. Noel, and M. F. Green, "Fatigue behavior of reinforced concrete beams with temperature differentials at room and low temperature," *Journal of Structural Engineering*, vol. 143, no. 7, Article ID 04017056, 2017.

[14] C. Gheorghiu, P. Labossière, and J. Proulx, "Response of CFRP-strengthened beams under fatigue with different load amplitudes," *Construction and Building Materials*, vol. 21, no. 4, pp. 756–763, 2007.

[15] M. Ekenel, A. Rizzo, J. J. Myers, and A. Nanni, "Flexural fatigue behavior of reinforced concrete beams strengthened with FRP fabric and precured laminate systems," *Journal of Composites for Construction*, vol. 10, no. 5, pp. 433–442, 2006.

[16] H. B. Zhu, *Method and Experiment Research on Highway Reinforced Concrete Simply-Supported Girder Bridge's Fatigue Residual Service Life Forecast*, Central South University, Changsha, China, 2011.

[17] Y. F. Ma, X. C. Su, Z. Z. Guo, L. Wang, and J. R. Zhang, "Experimental study on fatigue behavior of reinforced concrete beams with corrosion-induced cracking," *Journal of Natural Disasters*, vol. 26, no. 6, pp. 61–68, 2017.

[18] X. F. Li, P. G. Wu, and G. Y. Zhao, "Experimental research on bending fatigue behavior of high-strength concrete beams," *China Civil Engineering Journal*, vol. 30, no. 5, pp. 37–42, 1997.

[19] GB 50010-2010, *Code for Design of Concrete Structures*, China Architecture & Building Press, Beijing, China, 2011.

[20] A. Soltani, K. A. Harries, B. M. Shahrooz, H. G. Russell, and R. A. Miller, "Fatigue performance of high-strength reinforcing steel," *Journal of Bridge Engineering*, vol. 17, no. 3, pp. 454–461, 2012.

[21] D. Y. Gao, M. Zhang, and H. T. Zhu, "Fatigue test and stiffness calculation of steel fiber reinforced high-strength concrete beams with reinforcements," *Journal of Building Structures*, vol. 34, no. 8, pp. 142–149, 2013.

[22] J. Schijve, *Fatigue of Structures and Materials*, Springer Press, Berlin, China, 2nd edition, 2013.

[23] X. F. Li, P. G. Wu, and G. Y. Zhao, "Experimental study on fatigue properties of deformed bars," *Engineering Mechanics*, vol. 14, no. sup1, pp. 349–356, 1997.

[24] Y. P. Song, *Fatigue Behavior and Design Principle of Concrete Structures*, China Machine Press, Beijing, China, 2006.

[25] S. Suresh, *Fatigue of Materials*, National Defense Industry Press, Beijing, China, 2nd edition, 1999.

[26] J. W. Fisher, *Effect of Weldments on the Fatigue Strength of Steel Beams (NCHRP Report 102)*, Transportation Research Board of the National Academies, Washington, DC, USA, 1974.

[27] PD 6695-1-9: 2008, *Recommendations for the Design of Structures to BS EN 1993-1-9*, BSI, London, UK, 2008.

[28] TB/T 2349-2016, *Fatigue Test Method for Connection of Railway Steel Bridge*, China Railway Press, Beijing, China, 2016.

[29] M. Zhong, H. L. Wang, Z. B. Liu, and J. W. Meng, "Experimental research of high-strength concrete beams reinforced by high-strength bars under static loading and fatigue loading," *Journal of Building Structures*, vol. 26, no. 2, pp. 94–100, 2005.

[30] C. EN. Eurocode 2, *Design of Concrete Structures – Part 1-1: General Rules and Rules for Buildings (EN 1992-1-1)*, BSI, London, UK, 2004.